

Modeling of relative permeabilities including dynamic wettability transition zones

Abay M. Kassa^{1,2} Sarah E. Gasda² K. Kumar¹ F. A. Radu¹

¹ Department of Mathematics, University of Bergen, P. O. Box 7800, 5020 Bergen, Norway.

² NORCE, Nygårdsgaten 112, 5008 Bergen, Norway.

Corresponding author: Abay M. Kassa (E-mail: abka@norceresearch.no)

Abstract

Wettability is a pore-scale property that impacts the relative movement and distribution of fluids in a porous medium. There are reservoir fluids that provoke the surface within pores to undergo a wettability change. This wettability change, in turn, alters the dynamics of relative permeabilities at the Darcy scale. Thus, modeling the impact of wettability change in the relative permeabilities is essential to understand fluids interaction in porous media. In this study, we include time-dependent wettability change into the relative permeability–saturation relation by modifying the existing relative permeability function. To do so, we assume the wettability change is represented by the sorption-based model that is exposure time and chemistry dependent. This pore-scale model is then coupled with a triangular bundle-of-tubes model to simulate exposure time-dependent relative permeabilities data. The simulated data is used to characterize and quantify the wettability dynamics in the relative permeability–saturation curves. This study further shows the importance of accurate prediction of the relative permeability in a dynamically altering porous medium.

1 Introduction

Wettability alteration (WA) plays an important role in many industrial applications such as microfluidics nanoprinting, enhanced oil recovery (EOR), and CO₂ storage [1, 2, 3, 4, 5]. Wettability refers to the tendency of one fluid over the others to spread on or adhere to a solid surface [35, 1] and is defined by the fluid–fluid contact angle (CA). This pore-scale property regulates the distribution of fluids in the pore spaces and controls the relative flow of immiscible fluids in a porous medium [38, 37, 35, 1]. This, in turn, impacts constitutive relations in the multi-phase flow systems such as residual saturation, relative permeability, and capillary pressure at the Darcy scale [36, 39, 40, 4, 35]. Investigating and upscaling the impact of WA on the constitutive relations (hereafter constitutive relations refers to the relative permeability- and capillary pressure-saturation relations) is of great importance.

Wettability is assumed to be static in time and uniform in space. However, wettability is a dynamic process that depends on surface chemistry, composition of fluids, exposure time, and reservoir conditions (pressure and temperature) to name a few [41, 42, 38, 11, 10, 9, 43]. Experiments on crude oil/brine/rock systems have shown that adsorption of active components from the crude oil is able to change the wettability of the sample porous medium from water-wet to intermediate-wet system [41, 44, 9]. It is also hypothesized that the oil reservoir may be more oil-wet than what is

observed from the experiment. This is because the adsorption time of the experiment period was much less than the age of the oil in the reservoir. Furthermore, CO_2 is one of the reservoir fluids which contain active components that can provoke the surface within the pores to undergo a WA [45, 46, 47, 48, 49, 50, 51, 52, 53, 4].

Generally, the WA process can have three phases that delineate the transition from initial to final wetting-state conditions, e.g. initial-wet, final-wet, and dynamic-wet. The end (initial and final) wetting conditions are static in time but can be uniform and mixed in space. A mixed-wet condition could be created by rock mineral and exposure history differences. This is due to the fact that a pore surface exposed to the WA agent may be altered to a new wetting condition, while the unexposed surface keeps the initial wetting state [54, 7]. This creates a mixed-wet condition even within a single pore and was observed and explained first by Salathiel et al. [41] in the 1970s. Usually, WA is assumed to occur instantaneously and is considered as a function of the WA agent concentration. In some cases, however, the alteration process might take prolonged time in the scale of weeks and months [14, 18, 9, 55]. In this regard, the dynamic-wet phase can be a function of exposure time in addition to the WA agent concentration.

The WA process may result in a saturation function alteration for subsequent drainage-imbibition displacements and thus cause hysteresis in constitutive relations [56, 36, 57, 58, 59]. For instance, core-flooding measurements for (supercritical or gas) CO_2 -water system have indicated that WA-induced alteration in the residual saturation and capillary pressure curves despite the fact that they were measured following a standard procedure, i.e., where “pressure equilibration” is obtained after each increment in pressure [17, 19, 14, 20, 45, 13]. In these measurements, a steadily change in capillary pressure function over time was observed. More importantly, the capillary pressure deviation from the initial-wet state curve could not be explained by classical scaling arguments. The instability and gradual change of residual saturation and capillarity through exposure time, in turn, impact the behavior of relative permeabilities.

The above experiments reveal that standard constitutive models are not well suited to predict relative permeability and capillary pressure under dynamic, long-term WA. One alternative is to use mixed-wet model, e.g. Kjosavik et al. [60] and Lomeland et al.[61], that capture the static heterogeneity of wettability in the relative permeabilities. The main feature of these models is their flexibility to describe hysteresis and scanning curves caused by a wettability gradient in space. Other alternatives are models designed to handle the instantaneous WA process in the relative permeabilities. The first class of these models involves a heuristic approach that interpolates between the initial and final wetting states in which the WA effect is captured as a coefficient function [25, 3, 27, 28, 62]. Interpolation models are conceptually simple, while the initial and final wetting states are characterized by standard functions, e.g. Brooks-Corey [63] or van Genuchten [64]). The other approach incorporates the effect of the instantaneous WA into the relative permeabilities through the residual saturation directly [26]. To date, only Al-Mutairi et al. [29] have considered the effect of time-dependent WA in both the relative permeabilities and capillary pressure functions explicitly. However, their model does not sufficiently incorporate or upscale the WA processes to core-scale laws.

Appropriate upscaling of the pore-scale time-dependent WA process connected to the capillary pressure function was the subject of our recent work [65]. There, WA dynamics were upscaled by introducing a mechanistic time-dependent CA model at the pore-level that was coupled with a cylindrical bundle-of-tubes model and used to simulate capillary pressure curves for drainage and imbibition displacements. The simulated data was used to formulate and quantify a interpolation-based capillary pressure model at the Darcy scale. The new dynamic model resolves the existing interpolation models used in the studies of reservoir simulation [28, 25, 3, 27, 62] by including the dynamics in time and quantifying the pore-scale WA process to the interpolation model in a

systematic manner.

One may consider employing a similar approach to [65] and an interpolation-type model to capture the pore-scale underpinnings of WA in the relative permeability behaviors. However, time-dependent WA may impact the capillary pressure and relative permeabilities in different ways. As observed in [65], WA has a direct impact on the entry pressure in each pore and reflects it at the Darcy scale. Furthermore, a small change in CA exerts a large impact on the dynamics of the capillary pressure function. However, the relative permeability alteration occurs when the WA affects the pore filling/draining orders of pore-sizes. This may lead to a longer exposure time to observe a relative permeability deviation from the initial-wet state curve. Furthermore, unlike the capillary function, the relative permeability curves are constrained between zero and one for any change of wettability. These features of the relative permeability may impact the modeling approach to upscale the pore-scale WA process to the relative permeability behavior.

To our knowledge, a physically reliable model to characterize a prolonged exposure time-dependent WA induced dynamics in the relative permeability behaviors has not been proposed yet. This paper revises and extends the approach discussed in [65] to develop a relative permeability model that includes pore-level time-dependent WA processes. Section 2 summarizes two possible approaches that can be applied to upscale the impact of time-dependent WA in the relative permeabilities. The fluid-fluid CA change is designed as a function of exposure time to the WA agent at the pore level to measure the WA process. This model is coupled with a pore-scale, triangular bundle-of-tubes, model to simulate time-dependent WA induced relative permeability curves. These curves are presented in Section 3 and are used to evaluate the modeling approaches hypothesized in Section 2.

2 Modeling and simulation approach

A time-dependent WA may introduce a dynamic term in the relative permeability–saturation ($k_{r\alpha}$ - S) relationship. This dynamic term can be measured by its deviation from the static initial wetting-state as:

$$k_{r\alpha}(\cdot) - k_{r\alpha}^i(S_\alpha) := f_\alpha^d(\cdot), \quad (1)$$

or, the dynamic term can be correlated with the parameters of the standard models

$$k_{r\alpha}(\cdot) = k_{r\alpha}^i(S_\alpha, a(\cdot), b(\cdot), \dots), \quad (2)$$

where $a(\cdot)$ and $b(\cdot)$ are fitting parameters that change along exposure time, whereas f_α^d represents the WA induced dynamic component, and the subscript $\alpha \in \{w, n\}$ represents the wetting and non-wetting phases.

In this study, we explore both approaches in Eqs. (1) and (2) to quantify and characterize f_α^d in the relative permeabilities for a system that undergoes a WA. From Equation (1), we propose an interpolation model following our previous work [65], where the dynamic component is designed to interpolate between two end wetting-state curves. To obtain an interpolation model, the dynamic component in Eq. (1) can be scaled by the difference between the initial and final wetting-state relative permeability curves. The resulting quantity is non-dimensional and referred to as the *dynamic coefficient*,

$$\omega_\alpha(k_{r\alpha}^f - k_{r\alpha}^i) = f_\alpha^d, \quad (3)$$

where the superscript i and f represents relative permeabilities at the initial and final wetting-states respectively. This can be substituted into Eq. (1) to obtain dynamic relative permeability models

$$k_{r\alpha} = (1 - \omega_\alpha)k_{r\alpha}^i + \omega_\alpha k_{r\alpha}^f, \quad (4)$$

where ω_α , the dynamic coefficient, is responsible for capturing the wettability dynamics at the macroscale. Similar model to Eq. (4) were employed to include the impact of instantaneous WA into the relative permeability curves [25, 3, 27, 28, 62].

The approach in Eq. (2) relies on a systematic inclusion of the dynamic term f_α^d into the relative permeability function through the model parameters. This can be done by formulating the parameters $a(\cdot)$ and $b(\cdot)$ as a function of exposure time and WA agent in similar fashion as ω_α . This approach is motivated by the fact that the parameters in the standard relative permeability models are adjusted to different values when wettability changes from one state to the other.

Both the initial and final wetting-state curves can be characterized fully by the well-known relative permeability models such as van Genuchten[64] or Brooks-Corey [63], Purcell [66], the LET model [61] or a model proposed by Kjosavik et al. [60]. For the sake of brevity, we focus on the Brooks-Corey (BC) and LET models in this study. The BC relative permeabilities can be derived by integrating the capillary pressure over the capillary tubes [34, 60]. After the integration of the BC capillary pressure, one can obtain relative permeabilities

$$k_{rw}^i = S_w^{a_w}, \text{ and } k_{rn}^i = (1 - S_w^{a_n})(1 - S_w)^{m_n}, \quad (5)$$

for the water-wet system and

$$k_{rw}^f = (1 - S_w^{a_w})(1 - S_n)^{m_w}, \text{ and } k_{rn}^f = S_n^{a_n}, \quad (6)$$

for a hydrophobic system (see [60]), here a_w, a_n, m_w , and m_n are data fitting parameters in which the subscripts w and n indicate the wetting and non-wetting surfaces. Particularly the m 's are known to be tortuosity exponents. In 2005, Lomeland et al. [61] have proposed relative permeability models with three parameters L, E, and T for two-phase flow system. Their correlation models read as:

$$k_{rw}^i = \frac{S_w^{L_w}}{S_w^{L_w} + E_w(1 - S_w)^{T_w}}, \text{ and } k_{rn}^i = \frac{(1 - S_w)^{L_n}}{(1 - S_w)^{L_n} + E_n S_w^{T_n}}, \quad (7)$$

where L_α, E_α , and T_α are data fitting empirical parameters. A detailed description and explanation of the parameters can be found in [61]. The important characteristics of the LET model (7) is its flexibility to predict the relative permeability curves for any type of wettability conditions. We note that the parameters, a and b , in Eq. (2) are associated with data fitting parameters in Eqs. (5)-(6) and (7).

The WA induced dynamics in $k_{r\alpha}$ - S relation should be characterized in a unified manner in order to evaluate the behaviors of $\omega_\alpha(\cdot)$, $a(\cdot)$, and $b(\cdot)$ along exposure time to the WA agent. The WA induced $k_{r\alpha}$ - S data can be measured from laboratory experiments. However, this approach is expensive in terms of time. Thus, we follow a theoretical approach in which we simulate time-dependent $k_{r\alpha}$ - S data from a pore-scale model.

2.1 Pore-scale model description

We employed a triangular bundle-of-tubes to represent the pore-scale model. Note that one can also use a simpler pore-scale model, i.e., a cylindrical bundle-of-tubes model, to characterize the impact of WA on $k_{r\alpha}$ - S relations. However, polygonal pores are advanced in the way that they can represent physical processes such as the establishment of mixed wettability within a single pore. This may lead to different fluid distributions within a pore, and establishment of non-wetting fluid layers in the corners of the pore space and drainage through layers [54, 67, 72].

A bundle-of-tubes model is a collection of capillary tubes with a distribution of radii as depicted in Fig 1. The tubes in Fig 1 are connected with the wetting (right with pressure P_r^{res} .) and non-

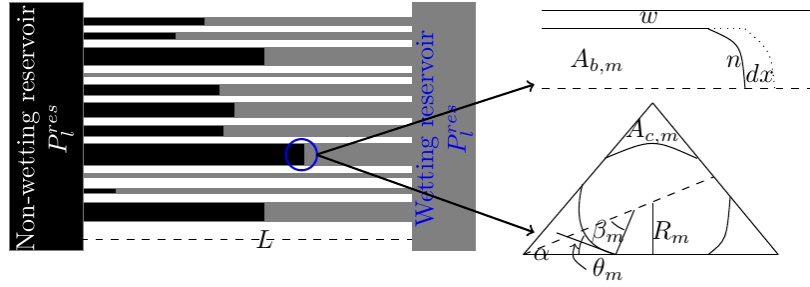


Figure 1: The fluid displacement scenario in a bundle of tubes that is connected with wetting and non-wetting phase reservoirs. The right column shows fluid distribution during primary drainage. For complete (drainage-imbibition cycles) fluid configurations, see Fig 2.

wetting (left with pressure P_l^{res} .) phase reservoirs. Once the fluid movement is initiated in the tubes, the fluid configurations in each tube can have the form as in Fig 1. Here, $A_{b,m}$, $A_{c,m}$, and dx represent the bulk area covered by the non-wetting fluid, the corner area still covered by the wetting phase, and change of fluids along the tube respectively, whereas α is half angle and θ_m is fluid-fluid CA. Detailed calculation of these areas and the angle β_m is discussed below.

Let the boundary pressures difference be defined as

$$\Delta P = P_l^{res} - P_r^{res}, \quad (8)$$

and the tubes in the bundle are filled with the wetting phase initially. To displace the wetting phase fluid in the m^{th} tube, the pressure drop has to exceed the local entry pressure [22]

$$\Delta P > P_{c,m}. \quad (9)$$

If condition (9) is satisfied, the non-wetting fluid starts to displace the wetting phase, and the volumetric flow rate in the m^{th} can be approximated by the Lucas-Washburn flow model [68],

$$q_m = \frac{\mathcal{G}_m(R_m, \theta_m)[\Delta P - P_{c,m}]}{8[\mu_{nw}x_m^{int} + \mu_w(L - x_m^{int})]}, \quad (10)$$

where, μ_{nw} and μ_w are non-wetting and wetting fluid viscosities, respectively, the superscript *int* stands for fluid-fluid interface, $q_m = dx_m^{int}/dt$ is the interface velocity, R_m is the m^{th} tube inscribed radius, and θ_m is the fluid-fluid contact angle at pore m . Here, θ_m is a general contact angle representation and can be specifically defined as $\theta_{r,m}$ if the interface is receding, $\theta_{a,m}$ if the interface is advancing, and $\theta_{h,m}$ if the interface hinges in the corner of the pores. The \mathcal{G}_m in Eq. (10) represents the conductance of the fluids and we follow the work of [67] to pre-compute the conductance. The interface is assumed to be trapped when it reaches the outlet of the tube, thus $q_m = 0$ when the interface reaches the boundaries.

The wettability change and/or gradient in the polygonal pores may create distinct fluid configurations, for example see Fig 2. These configurations can be encountered during drainage (e.g. A, D, and E) and imbibition (e.g. B, C, and F) displacements in each pore in the bundle. The bold surface in configurations B through F is to show that part of the surface is exposed to a WA agent at some point and experiences a wettability change. Configuration B occurs when the wettability is altered up to a CA value satisfying $\theta < \frac{\pi}{2} - \alpha$, where $\alpha = \frac{\pi}{6}$ is the corner half-angle and configuration C otherwise. Configuration F may occur when the non-wetting fluid invades configuration E. This is the case when the receding CA is sufficiently smaller than the previous advancing contact angle.

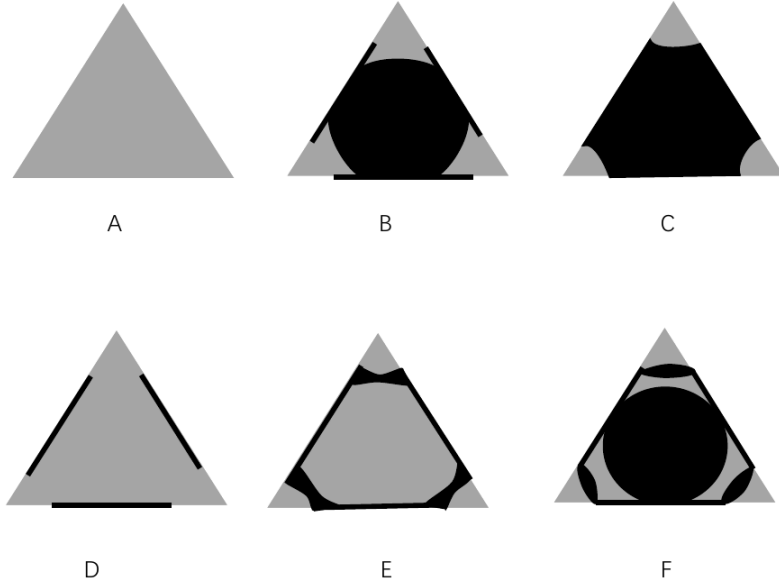


Figure 2: Fluid configurations for primary drainage, imbibition, and secondary drainage (water in light color and CO₂ in a dark color). We adopted the configurations from [72]. The bold lines along the sides indicate altered wettability.

Below, relevant aspects of the polygonal pores for the relative permeabilities measurement will be stressed, which includes entry pressure and the areas covered by the two fluids. The capillary pressure at the pore-level is given by

$$P_{c,m} = p_n - p_w = \frac{\sigma}{r_m}, \quad (11)$$

where p_n and p_w are the non-wetting and wetting phase pressures respectively, r_m is radius of arc meniscus (AMs) that separates the bulk from the corner fluid, and σ is fluid-fluid interfacial tension. The radius of curvature r_m is determined from the minimization of Helmholtz free energy of the system [69]. For isothermal, constant total volume, constant chemical potentials, and incompressible system, the minimization of the change in Helmholtz free energy can be simplified to [69, 43, 70]

$$P_{c,m}dV_n = \sigma(dA_{nw} + \cos(\theta_m)dA_{ns}), \quad (12)$$

where θ_m is fluid-fluid surface angle, dV_n is the change of non-wetting fluid volume, dA_{nw} , and dA_{ns} represent the change in area of fluid-fluid and fluid-solid interfaces respectively. In [72, 71, 74] the entry pressure curvature, r_m , and the fluid layer existence criterion were calculated from Eqs. (11) and (12) for each of the configurations in Fig 2. Here, we follow and implement the work of [72] to calculate the radius of curvature r_m and the associated entry pressure.

Once we obtained r_m for the m^{th} tube, fluid volumes (the bulk and corner fluids) can be calculated in terms of r_m and θ_m . To calculate these quantities, we numbered the fluid-fluid interfaces in order from the apex if there exist more than one interface in the corner, and we apply the indicator notation

$$I^k = \begin{cases} 1, & \text{if interface } k \text{ separates bulk nonwetting and corner water} \\ -1, & \text{if interface } k \text{ separates bulk water and corner nonwetting.} \end{cases} \quad (13)$$

The bulk cross-sectional area $A_{b,m}^k$ in each tube in the bundle is defined as,

$$A_{b,m}^k = \begin{cases} \frac{3R_m^2}{\tan \alpha} - 3r_m b_m^k \sin(\beta_m^k + \alpha) + 3r_m^2 \beta_m^k, & \text{if } I^k = 1, \\ \frac{3R_m^2}{\tan \alpha} - 3r_m b_m^k \sin(\beta_m^k - \alpha) - 3r_m^2 \beta_m^k, & \text{if } I^k = -1, \end{cases} \quad (14)$$

where

$$b_m^k = \frac{r \sin(\beta_m^k)}{\sin(\alpha)}, \text{ and } \beta_m^k = \begin{cases} \frac{\pi}{2} - \alpha - \theta_m^k & \text{if } I^k = 1 \\ \frac{\pi}{2} + \alpha - \theta_m^k & \text{if } I^k = -1. \end{cases} \quad (15)$$

Though we used a general notation for CA θ_m^k above, θ_m^k may be replaced by, $\theta_{r,m}$ and $\theta_{a,m}$ when the interface recedes and advances respectively, and $\theta_{h,m}^k$ if the interface, separating the bulk and corner fluids, is hinging. The hinging contact angle (if exists) changes with the entry pressure $P_{c,m}$ according to:

$$\theta_{h,m}^k = \begin{cases} \arccos\left(\frac{P_{c,m} b_m^k \sin(\alpha)}{\sigma}\right) - \alpha & \text{if } I^k = 1 \\ \arccos\left(\frac{P_{c,m} b_m^k \sin(\alpha)}{\sigma}\right) + \alpha & \text{if } I^k = -1. \end{cases} \quad (16)$$

The fluid area that occupies the corner regions can be estimated by

$$A_{c,m}(\theta_m) = 3r_m^2 \left(\theta_m + \alpha - \frac{\pi}{2} + \cos(\theta_m) \left(\frac{\cos(\theta_m)}{\tan(\alpha)} - \sin(\theta_m) \right) \right), \quad (17)$$

where θ_m is an argument to determine the appropriate area. The corner surface covered by water in configuration C is obtained by $A_{c,m}(\theta_{h,m}^1)$, whereas the non-wetting fluid layer in configuration E is calculated from $A_{c,m}(\pi - \theta_{a,m}) - A_{c,m}(\theta_{h,m}^1)$. The same approach can be applied if there exist many layers in the corner of the pore.

As clearly seen above the areas, $A_{b,m}$ and $A_{c,m}$ are dependent on wettability, i.e., fluid-fluid CA. For example, fluid configuration C and D occurs only if the condition $\theta_m \leq \frac{\pi}{2} - \alpha$ is satisfied during the drainage displacement. Otherwise, the non-wetting phase occupies the cross sectional area of the tube, and the entry pressure calculation is reduced to the well known Young-Laplace equation. On the other hand, the non-wetting fluid layer occurs in the corner when the condition $\theta_m > \frac{\pi}{2} + \alpha$ is satisfied. This implies that a dynamic change of CA can also determine the fluid distribution in a single pore.

2.2 Pore-scale time-dependent wettability model

Above, we observed that the entry pressure in Eq. (12), fluid distributions in Eqs. (14)-(17), and a conductance in Eq. (10) are wettability evolution dependent. In this section, we introduce a WA mechanism at the pore level to examine its impact on the saturation distribution. We recall that there are many factors that provoke the surface within the pore to undergo a wettability change. Here, we consider the effect of exposure time and fluid-history on the CA change with the assumption that:

- The CA of the pore surface is altered through exposure time to the WA agent and the alteration is permanent. That means the wettability is not restored to the original wetting condition when the WA agent is displaced by the other fluid unless the displacing fluid has a composition that gradually restores the original wetting condition.

- The WA becomes quasi-static in time if the WA agent is removed from the pore before the final wetting-state is reached. If the agent is reintroduced at some later point, alteration continues until the final state.

According to the assumptions above, the bulk surface area $A_{b,m}$ is supposed to be altered dynamically in time, whereas the corner surface area $A_{c,m}$ may keep the initial condition. Thus, we introduce a functional form to describe a WA mechanism for any arbitrary tube m as

$$\theta_m(\cdot) := \begin{cases} \theta_m^i & \text{for } A_{c,m}, \\ \theta_m^i + \varphi(\cdot)\Delta\Theta & \text{for } A_{b,m}, \end{cases} \quad (18)$$

where $\Delta\Theta = \theta_m^f - \theta_m^i$, θ_m^f , θ_m^i are the final and initial contact angles respectively. The WA model (18) is designed to evolve from an arbitrary initial wetting state to the final wetting condition so that φ is used to interpolate between end wetting conditions and has a value between zero and one.

Theoretical investigation and detailed laboratory measurement on time-dependent WA is very limited. Furthermore, WA is a complex process, where surface free energies, surface mineralogy, fluid composition and exposure time interact. However, adsorption of the WA agent onto the surface area is a natural process in CA change. Such adsorption type wettability evolution is observed for CA measurements [48, 50, 49, 75, 77, 76]. These all give an insight to model φ in Eq. (18) according to the adsorption of the WA agent and can be given as follows

$$\varphi := \frac{\chi_m}{C + \chi_m}, \quad (19)$$

where C is a non-dimensional parameter that controls the speed and extent of alteration from initial-wet to final-wet system. The derivation of Eq. (19) can be found in our previous work [65]. The variable χ_m is a measure of exposure time and is defined as

$$\chi_m := \frac{1}{T} \int_0^t \frac{A_{b,m} x_m^{int}}{V_{p,m}} d\tau, \quad (20)$$

where T is a pre-specified characteristic time, x_m^{int} is the fluid-fluid interface position along the tube length L , $A_{b,m}$ is the pore surface area that covered by the non-wetting fluid, and $V_{p,m}$ is the pore volume. Without losses of generality, the characteristic time T is set to be the time for one complete drainage displacement under static initial wetting condition, which can be pre-computed from Eq. (10).

For a given interface position x_m^{int} , one can determine the required time to reach the specified interface position from Equation (10). The obtained time is used in Eq. (20) to calculate the exposure history of the m^{th} pore to the WA agent. According to Eq. (20), each individual pore surface area $A_{b,m}$ will experience CA change based on the exposure time to the altering fluid, which may be different for different pores depending on the local saturation history. This process would give rise to a *non-uniform* wetting condition across the bundle until all pores have reached the final wetting-state. Moreover, the bulk surface area $A_{b,m}$ is the only surface that undergoes WA, and the corner surface area that covered by water is not subject to WA. This results in mixed-wet condition. However, this paper does not consider the wettability gradient across the length of the tubes because the time to drain is assumed to be fast compared to the exposure time for WA to occur.

2.3 Simulation approach

The wettability dynamics described in Eq. (18) are coupled into a triangular bundle-of-tubes model to simulate relative permeability curves according to Algorithm 1. Here, the relative permeability

for phase α is calculated as

$$k_{r\alpha} = \frac{Q_\alpha \mu_\alpha L}{\mathcal{K} A_T \Delta P_\alpha}, \quad (21)$$

where Q_α is the volumetric total flow rate of phase α , \mathcal{K} is absolute permeability of the bundle, A_T is the cross-sectional area of the bundle. We have repeated algorithm 1 for a few numbers of

Algorithm 1 A single drainage-imbibition cycle. Fluid and rock properties are given according to Table 2

```

1:
2: Drainage displacement
3:
4: Set  $P_c^{\max}$  % the maximum capillary pressure
5: while  $\Delta P < P_c^{\max}$  do
6:   Calculate  $P_c$  from Eq. (12)
7:   if  $\Delta P > P_c$  then
8:     Calculate  $S_{nw}$  and  $\bar{\chi} = \frac{1}{T} \int_0^t S_{nw} d\tau$ 
9:     Calculate  $K_{r\alpha}$ 
10:    Update  $\theta_m$  from Eqs. (18) and (20)
11:   end if
12:   Increase  $\Delta P$ 
13: end while
14:
15: Imbibition displacement
16:
17: Set minimum entry pressure  $P_c^{\min}$ 
18: while  $\Delta P > P_c^{\min}$  do
19:   Calculate  $P_c$  from Eq. (12)
20:   if  $\Delta P < P_c$  then
21:     Calculate  $S_{nw}$  and  $\bar{\chi}$ 
22:     Calculate  $K_{r\alpha}$ 
23:     Update  $\theta_m$  from Eqs. (18) and (20)
24:   end if
25:   Increase  $\Delta P$ 
26: end while

```

drainage-imbibition cycles provided that the WA process is completed within these displacements. The flow rate (or the pressure drop ΔP) is controlled in an arbitrary manner in order to gain θ^f for each tube within a few numbers of drainage-imbibition cycles. When we reduce the increment of each ΔP , the flow rate becomes very slow. This imposes a prolonged exposure to the WA agent and thus χ_m grows and eventually results in a large change in CA. For example, each ΔP increment is reduced by three order of magnitude for the last cycle compared to the first cycles to complete the alteration process.

The relative permeabilities–saturation “data points” are obtained in each drainage-imbibition cycle, and the obtained data is presented in the following Section. The generated $k_{r\alpha}$ - S curves are used to quantify the dynamics in the relative permeabilities which caused by time-dependent WA. The goal is to develop a correlation model that involves only a few parameters. Finally, the relation between these parameters and changes in the pore-scale WA model parameter C is studied and examined.

3 Simulation results

The two-phase flow simulation tool at the pore-scale (Algorithm 1) is implemented in MATLAB. The pore-scale model consists of parallel triangular tubes that connect the non-wetting and wetting reservoirs. Each tube in the bundle is assigned a different radius R , with the radii drawn from a truncated two-parameter Weibull distribution [67]

$$R = (R_{\max} - R_{\min}) \left\{ -\delta \ln \left[x(1 - \exp(-1/\delta)) + \exp(-1/\delta) \right] \right\}^{1/\gamma} + R_{\min}, \quad (22)$$

where R_{\max} and R_{\min} are the pore radii of the largest and smallest pore sizes respectively, and δ and γ are dimensionless parameters. The rock parameters and fluid properties are listed in Table 1. These parameters are coupled to the bundle-of-tubes model to simulate fluid conductance and

parameters	values	unit	parameters	values	unit
σ	0.0072	N/m	no. radii	500	[-]
R_{\min}	1	μm	R_{\max}	100	μm
θ_m^f	180	degree	θ_m^i	0.0	degree
μ_w	0.0015	Pa.s	μ_{nw}	0.0015	Pa.s
L	0.001	m			
δ	1.5	[-]	γ	0.5	[-]

Table 1: Parameters used to simulate quasi-static fluid displacement in a bundle-of-tubes.

relative permeability curves. In the following section, we present and discuss the simulated relative permeability and related results.

3.1 End wetting-state relative permeability

In section 2, we point-out that end wettingstate relative permeabilities are the foundation to characterize the dynamic relative permeability curves. Thus, it is natural to examine the end-state $k_{r\alpha}$ - S relations before quantifying the dynamic relative permeabilities using the same pore-size distribution and fluid properties in Table 1. Thus, we simulated static $k_{r\alpha}$ - S data by fixing the wettability at pre-specified initial θ_m^i and final θ_m^f values in each tube, see Table 1. The simulated curves are plotted along the saturation path in Fig 3.

We correlated both the BC (in Eqs. (5)-(6)) and LET (in Eq. (7)) models with the simulated (initial and final wetting-state) static $k_{r\alpha}$ - S curves, and the result is compared in Fig 3. The fitted parameters for the correlation models are found in Table 2. Both the BC correlations and LET models give an excellent match to the simulated phase relative permeability curves under static conditions.

As a complement, we have done experiments on the sensitivity of model parameters (not shown here) for different pore-size distributions by setting the wetting condition to be static. In this experiment, we found that the parameters L_n and T_w in the LET model can be unity for any pore-size distribution. Furthermore, from the end wetting-state correlation results, we observe that E_α is the only parameter that depends on wettability change, whereas the BC model parameters are sensitive for wettability change, see Table 2. More importantly, we have noticed that the parameters L_w and T_n have the same value and thus, we can represent them with a single parameter (say λ). Furthermore, the parameter E_n is the inverse of E_w . In this regard, we can reduce the LET model

Model	Parameters	Initial value (θ^i)	Final value (θ^f)
BC	a_w	0.9	1.839
	m_w	0.7329	0
	a_n	1.65	0.908
	m_n	0.075	0.7329
LET	L_w	1.3	1.3
	E_w	2.08	0.3
	T_w	1	1
	L_n	1	1
	E_n	0.48	3.37
	T_n	1.3	1.3

Table 2: Estimated correlation parameter values for initial and final wetting-state relative permeability curves.

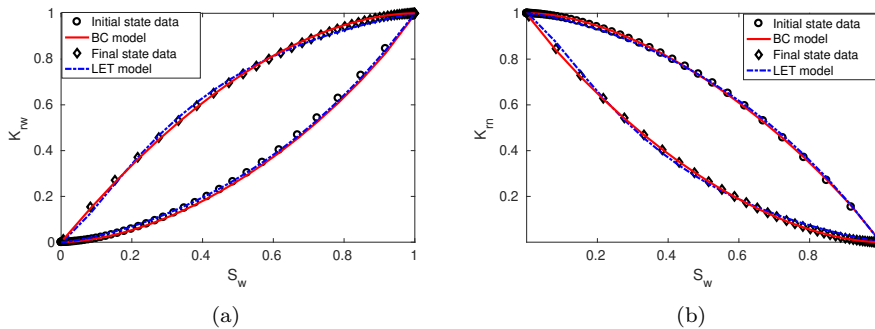


Figure 3: The BC and LET correlation models compared to the initial and final wetting-state relative permeability curves: (a) wetting phase and (b) non-wetting phase relative permeabilities.

to a two-parameter (but in each phase) model and we call it *reduced LET* model which read as

$$k_{rw} = E_n S_w^\lambda (E_n S_w^\lambda + 1 - S_w)^{-1}, \text{ and } k_{rn} = (1 - S_w)(1 - S_w + E_n S_w^\lambda)^{-1}. \quad (23)$$

The model in Eq. (23) is a two parameter model with only one parameter that varies along the wettability change. This makes the reduced LET model more reliable than its counter part, i.e., the BC model. Note that the parameter λ can also vary with wettability. In this case, a better match with the simulated relative permeability data can be obtained.

3.2 Simulated relative permeabilities

We demonstrate five drainage-imbibition cycles and simulate dynamic $k_{r\alpha}$ - S relations in each cycle (see Fig 4), while the tubes in the bundle are altered through time (see Fig 5) following the CA model (18). These data are generated with a pore-scale parameter $C = 10 \times 10^{-5}$. Note that the CA change may be halted (temporarily) in the pores if the displacement is to configuration D after imbibition. In this case, the drainage curve may follow the previous imbibition path. However, the

imbibition curve may show a deviation from the previous drainage curve if wettability is altered sufficiently.

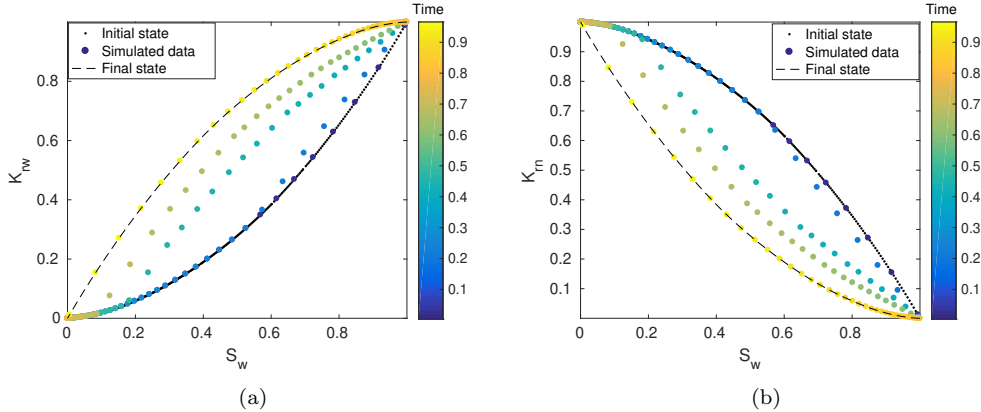


Figure 4: Simulated dynamic relative permeability curves ((a) wetting phase and (b) non-wetting phase) with respect to wetting phase saturation. The static $k_{r\alpha}$ - S curves for the initial and final wetting states are shown as a reference. The color code shows the $k_{r\alpha}$ - S dynamics within a year of exposure time.

According to the CA distribution in Fig 5 and $k_{r\alpha}$ - S curves in Fig 4, the wettability that ranges from strongly to weakly water-wet does not affect the pore filling and draining orders of the pore-sizes. As a consequence, the $k_{r\alpha}$ - S relations for drainage/imbibition displacements follow the same saturation path of the initial-wet condition. This implies that a WA induced $k_{r\alpha}$ - S hysteresis may not occur in a straight bundle-of-tubes model for a wettability range of $0^\circ \leq \theta_m \leq 60^\circ$. Similar $k_{r\alpha}$ - S relations are reported for a pore-network model with a wettability range of $\theta_m = 0^\circ$ to 45° [36]. This is in contrast to the capillary pressure–saturation relation, where a small change of CA impacts the P_c - S path significantly [65]. However, imbibition/drainage displacement may not necessarily occur in monotonically increasing/decreasing order of pore-sizes when the wettability of the pores (some) are altered to intermediate/weakly hydrophobic. This results in a relative permeability–saturation path deviation as observed in Fig 4.

We observe that the wetting and non-wetting phase relative permeabilities steadily increase and decrease (see Fig 4) respectively in each subsequent drainage-imbibition displacements when the wettability evolves from hydrophilic to hydrophobic conditions. This occurs because the relatively larger pores start allowing the water (originally wetting phase) to imbibe through before the smaller pores when the medium is altered to intermediate/hydrophobic system. On the contrary, the originally non-wetting fluid prefers the smaller pores to flow in during drainage. As a consequence, a mobility reduction and improvement respectively for the non-wetting and wetting phase relative permeabilities are observed. However, any additional drainage-imbibition cycle would follow along the static curve for the final wetting state once the final CA (θ^f) is reached.

Analogous to the capillary pressure–saturation relation [65], time-dependent WA introduces dynamic hysteresis in the $k_{r\alpha}$ - S relations for a bundle-of-tubes model as shown in Fig 4. The $k_{r\alpha}$ - S hysteresis imposes a non-unique relation between the relative permeabilities and saturation. This is one of the challenging features of WA during the quantification of the dynamics in relative permeabilities. To eliminate the hysteresis observed in the $k_{r\alpha}$ - S relation, we projected the simulated relative permeability data onto the temporal domain $\bar{\chi}$ in Fig 7. The temporal domain, $\bar{\chi}$ is the

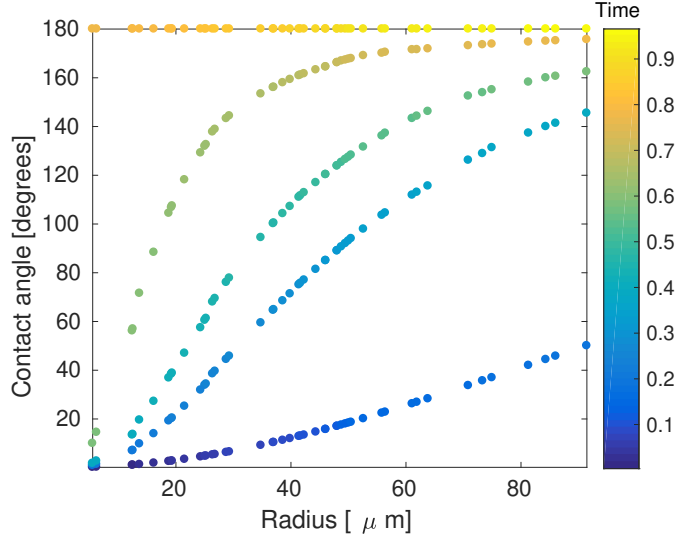


Figure 5: Dynamic CA evolution as a function of exposure time to the WA agent per each tube. This CA distribution was recorded at the end of each drainage-imbibition cycle and the color code shows the CA dynamics during a year of exposure time.

measure of the exposure history in averaged sense which defined as:

$$\bar{\chi} = \frac{1}{T} \int_0^t S_{nw} d\tau. \quad (24)$$

Unlike $k_{r\alpha}-S$, $k_{r\alpha}-\bar{\chi}$ is uniquely related but non-monotonically i.e., it raises to one and decreases to zero in time along each drainage-imbibition cycle.

The WA process also affects the corner fluid distribution in each drainage/imbibition displacement. Fig 7 shows the evolution of (average) corner wetting and non-wetting saturations. The wetting phase saturation decreases through time while the layer saturation grows. This is because wettability is altered from water-wet to hydrophobic and thus, the originally non-wetting fluid prefers to be in the corners. However, when (all) pores become more hydrophobic, the corner water increases and bulges-out during imbibition. This process may result in a layer collapse and has shown in the fifth imbibition, where the layer saturation increases during larger pores were imbibed and decrease when smaller pores imbibed over exposure time. Here, we have checked the establishment of corner fluids during the calculation of $k_{r\alpha}-S$ relations in each drainage-imbibition displacements.

3.3 Dynamic relative permeability model development

The interpolation approach, similar to Eq. (4), was applied successfully to capture time-dependent WA mechanisms in the capillary pressure curves [65]. Thus, it is important to test the potential of the interpolation-based model (in Eq. (4)) to predict time-dependent dynamics in $k_{r\alpha}-S$ relation. The dynamic coefficient ω_α is calculated according to Eq. (2) and plotted in Fig 8. In Fig 8b, we observe that the dynamic coefficient ω_α is related to the exposure time $\bar{\chi}$ non-monotonically. Thus, it is challenging to propose a functional relationship between ω_α and $\bar{\chi}$ directly. On the other hand, the dynamic coefficient ω_α in Fig 8a is increasing with respect to the exposure time to the WA agent.

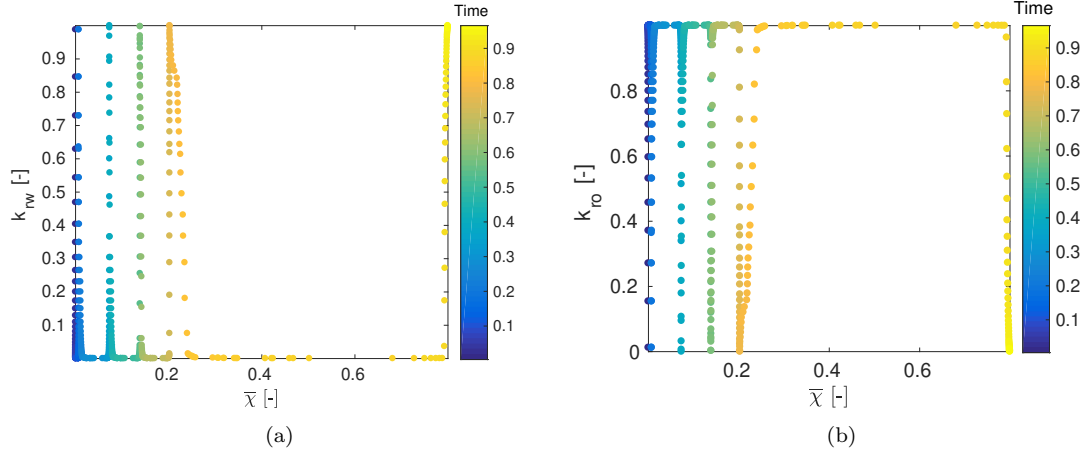


Figure 6: The relative permeability data: (a) wetting phase relative permeability and (b) non-wetting phase relative permeability as a function of $\bar{\chi}$ for the non-uniform WA case. The color of each data point indicates the time elapsed in years.

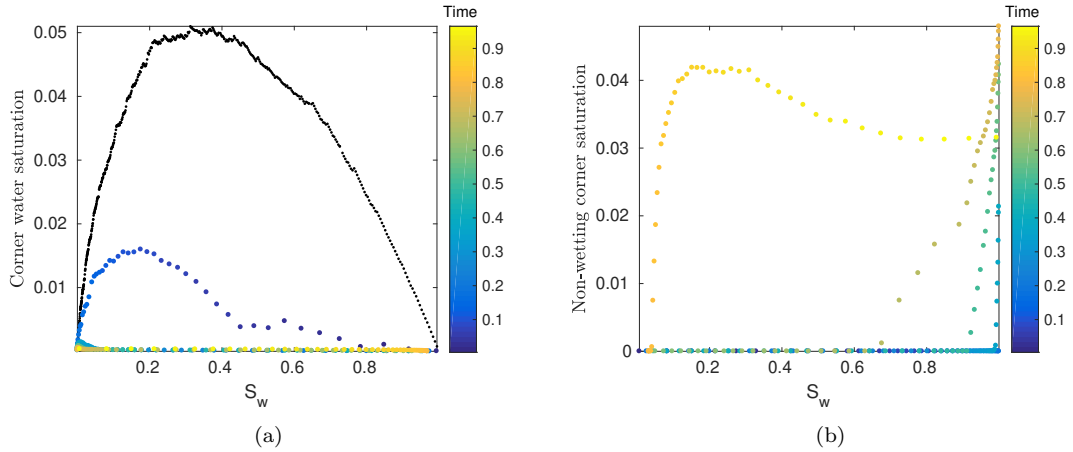


Figure 7: Corner fluid saturations: (a) wetting phases saturation and (b) non-wetting phase saturation. The color of each data point indicates the time elapsed in years.

However, the ω_α - S curves in Fig 8a have piece-wise functional forms i.e., zero and Langmuir-type function of phase saturation, that are altered with exposure time. This imposes another challenge to find a smooth model to predict the curves along with the saturation. But, one can design a piece-wise function to correlate the $\omega_\alpha - S$ data. From Fig 8a, we observe that the starting point of the Langmuir functional form is exposure time-dependent along the saturation path. Thus, the $\omega_\alpha - S$ can be represented as,

$$\omega_\alpha(S_w, \bar{\chi}) := \begin{cases} \frac{S_w - S_w^*(\bar{\chi})}{S_w - S_w^*(\bar{\chi}) + \beta(\bar{\chi})}, & \text{for } S_w > S_w^*(\bar{\chi}), \\ 0, & \text{otherwise} \end{cases} \quad (25)$$

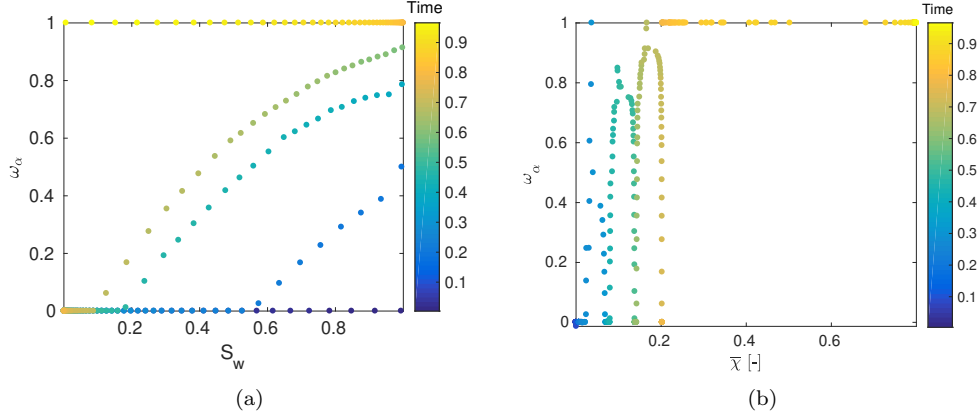


Figure 8: The scaled dynamic deviation from the initial wetting-state relative permeability curves as a function of wetting phase saturation (a) and exposure time $\bar{\chi}$ (b).

Parameter	Vale	Parameter	Value
a_1	0.0006123	a_2	0.001547
b_1	-2.522	b_2	-2.086
c_1	0.1297	c_2	0.2007

Table 3: The estimated parameter values for the interpolation model.

where S_w^* and β are time-dependent. The variable S_w^* is used to transform the starting point of the Langmuir part ω_α along the saturation to zero, and β is used to determine the curvature of the curve. From Fig 8a, we observe that the parameters S_w^* and β are decreasing functions of exposure time, $\bar{\chi}$.

We matched the designed model in Eq. (25) with the dynamic coefficient data, $\omega_\alpha - S_w$, to describe the relations $S_w^* - \bar{\chi}$ and $\beta - \bar{\chi}$. The obtained relations have the form,

$$S_w^* = a_1 \bar{\chi}^{b_1} + c_1, \text{ and } \beta = a_2 \bar{\chi}^{b_2} + c_2, \quad (26)$$

where a_i , b_i and c_i for $i = 1, 2$ are dimensionless fitting parameters. These parameters are estimated and given in Table 3 for this particular simulation.

The models in Eqs. (25)-(26) are then substituted back into the interpolation model (4) to give the dynamic relative permeability model and is read as,

$$k_{r\alpha} = \begin{cases} \frac{S_w - S_w^*(\bar{\chi})}{S_w - S_w^*(\bar{\chi}) + \beta(\bar{\chi})} (k_{r\alpha}^f - k_{r\alpha}^i) + k_{r\alpha}^i, & \text{for } S_w > S_w^*(\bar{\chi}) \\ k_{r\alpha}^i, & \text{otherwise.} \end{cases} \quad (27)$$

The dynamic model (27) is compared with the simulated relative permeability in Fig 9. According to Fig 9, the designed model predicts beyond the initial wetting state at joint-point of the initial wetting-state model and the designed interpolation model. This shows that the designed model (27) is badly correlated with the simulated $k_{r\alpha}$ - S data. Furthermore, the non-smoothness behavior of $\omega_\alpha - S_w$ results in a piece-wise phase relative permeability model with many dynamic parameters to be calibrated.

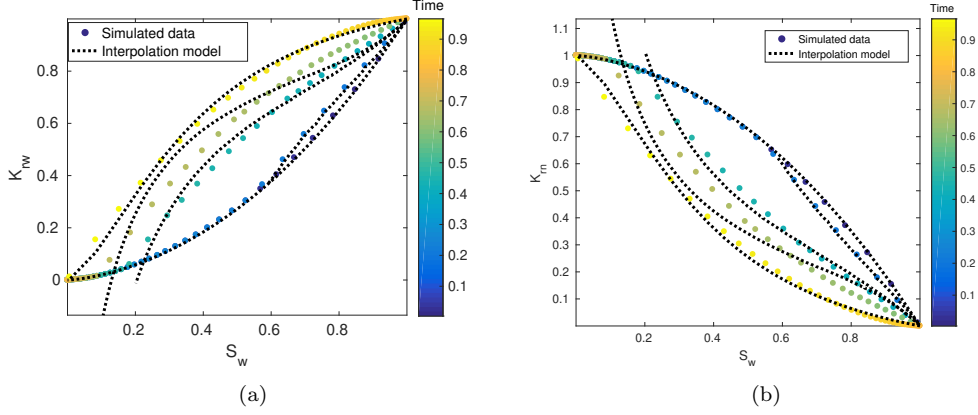


Figure 9: Comparison of the interpolation model (27) with the simulated (wetting (a) and non-wetting (b)) relative permeabilities.

The second approach discussed in Section 2 relies on establishing a relation between the model parameters and $\bar{\chi}$ to upscale the effect of pore-scale wettability evolution in relative permeabilities. This is supported by the result reported in Table 2 for end wetting-state curves in which the model parameters are dependent on the wetting condition of the porous domain in addition to the pore-size distribution. As a consequence, we can formulate dynamic correlation models from standard $k_{r\alpha}$ - S relations, i.e., BC models in Eqs. (5)-(6) or reduced LET models in Eq. (23). So far, we noticed that only E_α is sensitive for wettability change in the reduced LET model, whereas both parameters are sensitive in the BC model (see Table 2). This implies that the BC model is more expensive than the reduced LET model to upscale the effect of WA on relative permeabilities. Thus, we choose the reduced LET model to represent the dynamic relative permeability curves. Here, we rearrange the reduced LET model as

$$k_{rw} = \frac{\mathcal{L}_n(\bar{\chi}, E_n)S_w^\lambda}{\mathcal{L}_n(\bar{\chi}, E_n)S_w^\lambda + 1 - S_w}, \text{ and } k_{rn} = \frac{1 - S_w}{1 - S_w + \mathcal{L}_n(\bar{\chi}, E_n)S_w^\lambda}, \quad (28)$$

where λ and E_n are determined from the initial wetting-state correlation. Here, \mathcal{L}_n is designed to change with CA. Thus, we coupled the reduced LET model (28) with curve fitting tool in MATLAB and matched with the $k_{r\alpha}$ - S data to study the functional dependencies between the \mathcal{L}_n and $\bar{\chi}$. The obtained relation is linear and has the form

$$\mathcal{L}_n(\bar{\chi}, E_n) = a_n\bar{\chi} + E_n, \quad (29)$$

where E_n is as given in Table 2 and a_n is dynamic fitting parameter for wetting and non-wetting phase relative permeabilities and determines the slope of the relative permeabilities along exposure time. For this particular simulation this parameter is estimated to be $a_n = 3.57$ for all dynamic drainage-imbibition cycles reported above. Now the dynamic term \mathcal{L}_n in Eq. (29) can be substituted into the reduced LET model (28) to give the dynamic relative permeabilities:

$$k_{rw} = \frac{(a_n\bar{\chi} + E_n)S_w^\lambda}{1 - S_w + (a_n\bar{\chi} + E_n)S_w^\lambda}, \text{ and } k_{rn} = \frac{1 - S_w}{1 - S_w + (a_n\bar{\chi} + E_n)S_w^\lambda}, \quad (30)$$

where the parameters E_n and λ are pre-determined from the initial wetting-state correlation. The proposed dynamic relative permeability models in Eq. (30) and the simulated $k_{r\alpha}$ - S data are com-

pared in Fig 10. From Fig 10, we observe that the proposed dynamic model (30) correlated well

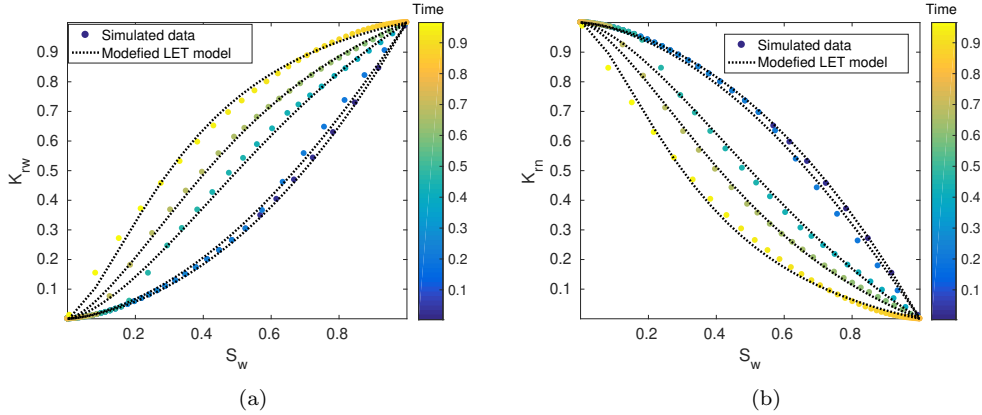


Figure 10: Comparison of the modified LET model and the simulated phase relative permeability: (a) wetting phase and (b) non-wetting phase.

with the simulated relative permeability curves. The proposed relative permeability model is single-valued regardless of the number of drainage-imbibition cycles. However, this single-valued model is not well predictive around the junction points, particularly for low wetting saturations. However, the obtained correlation result shown in Fig 10 is acceptable and a significant improvement on the interpolation model result shown in Fig 9. Furthermore, the modified LET model prediction can be improved by letting the parameter λ to vary along the exposure time. However, this may (at least) double the number of parameters in the model that need to be calibrated.

If we compare the two dynamic models (i.e., the piece-wise interpolation model in Eq. (27) and the reduced/modified LET model in Eq. (30)), the reduced LET model is more efficient and simpler to implement in the Darcy flow than the piece-wise interpolation model. Because, the reduced LET model is smooth along time and saturation. We also note that the number of parameters in the modified relative permeability model in Eq. (30) is reduced by half from the original LET model. These all make the reduced dynamic model more reliable than using a model consisting of multiple parameters that change in each cycle (or hysteresis models). Thus the analysis below will concern only on the modified LET model.

3.3.1 The modified LET model sensitivity to pore-scale model parameter

In this section, we will investigate the response of the upscaled model parameter a_n to the change in the CA model parameter C in Eq. (18). The parameter C controls the extent of WA at the pore-level, whereas a_n determines the WA induced dynamics in the relative permeabilities. We have simulated different drainage-imbibition $k_{r\alpha}$ - S curves by varying C to draw a relation between a_n and C . To do so, we determine the parameter a_n from each $k_{r\alpha}$ - S data that was simulated by considering different values of C . Then, we correlate the estimated parameter values of a_n with the chosen values of C , which can be read as

$$a_n = P_1 C + P_2, \quad (31)$$

where P_1 and P_2 are fitting parameters. The correlation result is plotted in Fig 11, where the parameters are estimated to be $P_1 = -18420$ and $P_2 = 6$. Therefore, we can predict the upscaled

dynamics of the relative permeabilities directly from the pore-scale WA process.

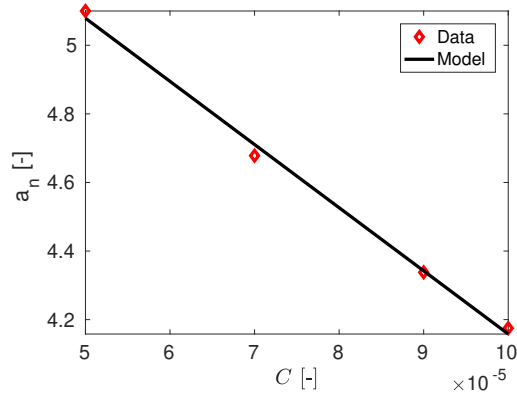


Figure 11: The relation between pore-scale wettability parameter C and the correlation parameter a_n in Eq. (30).

The relation in Eq. (31) can be substituted into the dynamic relative permeability model (30) to complete the upscaling process. The resulting dynamic relative permeability models are saturation, exposure time, and pore-scale WA parameter dependent. The pore-scale parameter has to be estimated from the calibration of CA model (18) with experimental data. Validating the underlying CA change model is beyond the scope of this paper. Rather, we consider the CA model as a reasonable basis to perform and analyze the upscaling process.

3.4 Applicability of the modified LET model to arbitrary saturation history

The saturation path that used to generate the relative permeability data in Fig 12 can be considered as one of the arbitrary paths in the domain $S_w \times \bar{\chi}$. This saturation path is dependent on the history of the exposure time to the WA agent (degree of WA change) and the reversal-point of saturation. This implies that the relative permeability-saturation dynamics may behave differently if one chooses a different saturation path that entails a prolonged exposure time for a fixed saturation profile and/or flow reversal at intermediate saturation.

Here, we simulate as many as possible $k_{r\alpha}$ - S curves that involve different reversal-points and exposure history within the $S_w \times \bar{\chi}$. Note that we use the pore-scale model parameter $C = 10 \times 10^{-5}$. The simulated data is plotted in Fig 12a and 12b for phase relative permeabilities. These arbitrary curves are used to test the potential of the modified LET model in Eq. (30). To do so, we apply the calibrated dynamic relative permeability model (30) to generate the $k_{r\alpha}$ - S - $\bar{\chi}$ surface. The absolute difference between the simulated data and the surface generated by the calibrated model is depicted in Fig 12c. According to the results in Fig 12, we can justify that a single saturation history path is sufficient to calibrate a dynamic model that can be applied to any saturation-time path.

3.5 Discussion

In contrast to the dynamic capillary pressure model presented in [65], the interpolation-based approach is poorly correlated with the simulated relative permeability curves. However, further in-

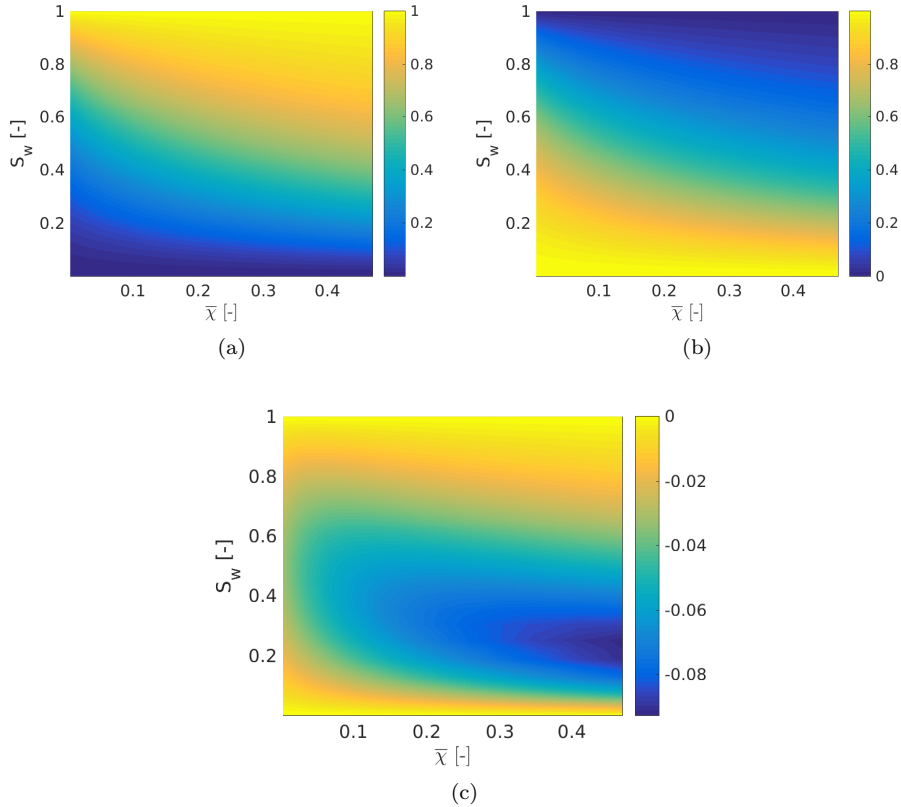


Figure 12: Top: Simulated relative permeabilities obtained by taking multiple paths in the $S_w \times \bar{\chi}$ space, for the wetting (left) and non-wetting (right) phases. Bottom: The difference between the dynamic model with the simulated data

investigation may be needed to re-evaluate the potential of capturing the WA process in the relative permeabilities based on the interpolation approach. We also examined the BC model to upscale the WA induced dynamics in the relative permeabilities though we do not report it here fully. For the sake of brevity, we have highlighted only the response of the BC model to the wettability change in Section 3.3 for end wetting conditions. In general, other models that involve more than two parameters (sensitive to CA change) could be calibrated with reasonable accuracy. But, these parameters need to be adjusted in each drainage-imbibition displacements. This complicates the modeling process and the resulting model may involve many parameters that may impose an extra challenge to analyze the WA impact on the flow dynamics at the Darcy scale.

In this study, we have developed a dynamic relative permeability model by modifying an existing static-wettability model i.e., the LET model. The original LET model consists of three parameters in each phase that need to be adjusted differently for different wetting conditions. First, we did numerical experiments to study the dependency of these parameters on the pore-size distribution, while the wettability was kept constant. We found that T_w for wetting and L_n for non-wetting phase relative permeability models are constant for any pore-size distribution. From this, we reduced the LET model to a model (the reduced model in Eq. (23)) that involves two parameters in each phase.

We further investigate the sensitivity of the reduced LET model parameters to the WA dynamics, and we found that only E_α is dependent on CA change dynamics. We then draw a clear relation between E_α and the exposure time $\bar{\chi}$ which allows us to come up with a single-valued dynamic relative permeability model that represents any arbitrary drainage-imbibition cycle. We note that the model involves two types of parameters. The first one is pore-size distribution dependent parameters E_n , L_w , and T_n which are determined *a priori* from the initial wetting-state correlation. Knowing these values, the parameter a_n is the only parameter that controls the WA induced dynamics in the relative permeabilities for both phases.

The proposed model is at the Darcy scale, that allows for a change in relative permeability as a function of averaged variables such as saturation (S_w) and exposure time to a WA agent ($\bar{\chi}$). This implies that the relative permeability in a grid block that is exposed to the WA agent may change over time even for constant saturation profile. However, if the grid block is not exposed to the WA agent, $\bar{\chi}$ is zero for this particular grid block. In this case, the dynamic model predicts the initial wetting-state curve. However, the developed model may continue further after the end wetting-state curve has attained which is in contrast to the interpolation-type model, where prolonged exposure does not contribute to the dynamics once the final wetting curve is met, see [65]. Thus it is important to propose a strategy to ensure that the relative permeability dynamics do not to cross the end-state curve. Above, the WA induced dynamics in the relative permeabilities is represented by

$$\mathcal{L}_n(\bar{\chi}) = a_n \bar{\chi} + E_n \quad (32)$$

where E_n is known from the initial wetting-state correlation. The final wetting state is attained when $a_n \bar{\chi} + E_n = E_n^f$ is satisfied. From this, we can estimate the exposure time needed to reach the final wetting state (say $\bar{\chi}_{\max}$) such that the relative permeability is represented by the end wetting-state curve. After knowing this we can set the dynamic variable as

$$\bar{\chi} = \begin{cases} \frac{1}{T} \int_0^t S_{nw} d\tau, & \text{if } \bar{\chi} < \bar{\chi}_{\max} \\ \bar{\chi}_{\max}, & \text{if } \bar{\chi} \geq \bar{\chi}_{\max} \end{cases} \quad (33)$$

This controls the unnecessary dynamics once the final wetting-state curve is predicted. Nevertheless, the dynamic term in the model pushes the relative permeability towards the higher and lower end of the curve for the wetting and non-wetting phases respectively.

Previous studies [25, 3, 27, 28] represent the impact of instantaneous WA on relative permeabilities by an interpolation model which matched directly to core-scale data in a heuristic manner. This study revealed that the interpolation model is not the best approach to upscale the pore-scale WA process. Rather, we have shown the potential of a modified LET model to capture the underlying WA process at the pore-scale represented by a triangular bundle-of-tubes. The proposed models are smooth and simple to use for practical applications. Most importantly, the models are designed to eliminate the relative permeabilities hysteresis induced by CA change during drainage and imbibition displacements. Similar to the developments in [65], we have quantified the link between the pore-scale model parameter C and the core-scale parameter a_n . We estimated the core-scale (dynamic) parameter a_n by varying the pore-scale parameter C . According to the simulation results, we have shown that a very simple scaling can relate a pore-scale process with the core-scale. This result implies that knowing the mechanism that determines the CA change at the pore-level can be used to predict the macroscale dynamics without performing pore-scale simulations. This is an important and valuable generalization for making use of experimental data to inform core-scale relative permeability-saturation relations.

4 Conclusion

In this paper, we developed a dynamic relative permeability model that includes the pore-scale underpinnings of WA in the relative permeability–saturation relationships at the Darcy scale. We found that the developed model (i.e., the modified LET model in Eq (28)) is simple to use and can predict WA induced changes in the relative permeabilities. The modified LET model shows a good agreement with the simulated relative permeability data. Furthermore, this model is independent of the saturation-time paths generated by any drainage-imbibition cycles. More importantly, the WA dynamics in the relative permeabilities is controlled by a single-valued parameter that has a clear relationship with the time-dependent CA change model parameter.

Acknowledgement

Funding for this study was through the CHI project (n. 255510) granted through the CLIMIT program of the Research Council of Norway.

References

- [1] BONN, D. & EGGERS, J. & HINDEKEU, J. & MEUNIER, J. & ROLLEY, E. 2009 Wetting and spreading. *Rev. Mod. Phys.* **81**, 739-805.
- [2] IGLAUER, S. & RAHMAN, T., & SARMADIVALEH, M. & AL-HINAI, A. & FERNØ, M. A. & LEBEDEV, M. 2016 Influence of wettability on residual gas trapping and enhanced oil recovery in three-phase flow: A pore-scale analysis by use of microcomputed tomography. *SPE J.* **21**, 1916–1929.
- [3] AU YU, L. & KLEPPE, H. & KAARSTAD, T. & SKJÆVELAND, S. M. 2008 Modelling of wettability alteration processes in carbonate oil reservoirs. *Netw. Heterog. Media* **3**, 149–183.
- [4] IGLAUER, S. & PENTLAND, C. H. & BUSCH, A. 2014 CO₂ wettability of seal and reservoir rocks and the implications for carbon geo-sequestration. *Water Resour. Res.* **51**, 729–774.
- [5] BLUNT, M. J. 2001 Flow in porous media– pore-network models and multiphase flow. *Curr. Opin. Colloid Interface Sci.* **6**, 197–207.
- [6] AHMED, A. & PATZEK, T. W. 2003 Impact of Wettability Alteration on Two-Phase Flow Characteristics of Sandstones: A Quasi-Static Description. *Water Resour. Res.* **39**, 1-12.
- [7] BLUNT, M. J. 1997 Pore Level Modeling of the Effects of Wettability. *SPE J.* **2**, 494–510.
- [8] MORROW, N. R. & LIM, H. T. & WARD, J. S. 1986 *Effect of crude-oil-induced wettability changes on oil recovery.* *SPE J.*, 89-103
- [9] BUCKLEY, J. S. & LIU, Y. & MONSTERLEET, S. 1988 Mechanisms of wetting alteration by crude oils. *SPE J.* **3**, 54-61.
- [10] Jadhunandan, P. P. & Morrow, N. R. 1995 Effect of Wettability on Waterflood Recovery for Crude-Oil/Brine/Rock Systems. *SPE Reservoir Engineering* **10**, 40–46.

- [11] HAAGH, M. E. J. & SIRETANU, I. & DUIJS, M. H. G. & MUGELE, F. 2017 Salinity-Dependent Contact Angle Alteration in Oil/Brine/Silicate Systems: the Critical Role of Divalent Cations. *Langmuir* **33**, 3349–3357.
- [12] SINGH, R. & MOHANTY, K. 2016 Foams with wettability-altering capabilities for oil-wet carbonates: A synergistic approach. *SPE J.* **21**, 1126–1139.
- [13] KIM, Y. & WAN, J. & KNEAFSEY, T. J. & TOKUNAGA, T. K. 2012 Dewetting of silica surfaces upon reactions with supercritical CO₂ and Brine: Pore-scale studies in micromodels. *Environ. Sci. Technol.* **46**, 4228–4235.
- [14] TOKUNAGA, T. K. & WAN, J. 2013 Capillary pressure and mineral wettability influences on reservoir CO₂ capacity. *Rev. Mineral. Geochem.* **77**, 481–503.
- [15] CHIQUET, P. & BROSETA, D. & THIBEAU, S. 2007a Wettability alteration of caprock minerals by carbon dioxide. *Geofluids*, 112–122.
- [16] CHALBAUD, C. & ROBIN, M. & LOMBARD, J. & MARTIN, F. & EGERMANN, P. & BERTIN, H. 2009 Interfacial tension measurements and wettability evaluation for geological CO₂ storage. *Adv Water Resour* **32**, 98–109.
- [17] PLUG, W. J. & BRUINING, J. 2007 Capillary pressure for the sand-CO₂-water system under various pressure conditions. Application to CO₂ sequestration. *Adv Water Resour* **30** 2339–2353.
- [18] WANG, S. & TOKUNAGA, T. K. 2015 Capillary pressure–saturation relations for supercritical CO₂ and brine in limestone/dolomite sands: Implications for geologic carbon sequestration in carbonate reservoirs. *Environ. Sci. Technol.* **49**, 7208–7217.
- [19] WANG, S. & TOKUNAGA, T. K. & WAN, J. & DONG, W. & KIM, Y. 2016 Capillary pressure-saturation relations in quartz and carbonate sands: Limitations for correlating capillary and wettability influences on air, oil, and supercritical CO₂ trapping. *Water Resour. Res.*, 6671–6690.
- [20] TOKUNAGA, T. K. & WAN, J. & JUNG, J. & KIM, T. W. & KIM, Y. & DONG, W. 2013 Capillary pressure and saturation relations for supercritical CO₂ and brine in sand: High-pressure $P_c(S_w)$ controller/meter measurements and capillary scaling predictions. *Water Resour. Res.*, **49**, 4566–4579.
- [21] HASSANIZADEH, S. & CELIA, M. & DAHLE, H. 2002 Dynamic effects in the capillary pressure–saturation relationship and its impacts on unsaturated flow. *Vadose Zone J* **1**, 38–57.
- [22] DAHLE, H. K. & CELIA, M. A. & HASANIZADEH, S. M. 2005 Bundle-of-Tubes Model for Calculating Dynamic Effects in the Capillary-Pressure Saturation Relationship. *Transport porous med* **58**, 5–22.
- [23] KRUMPFER, J. W. & MCCARTHY, T. J. 2010 Contact angle hysteresis: a different view and a trivial recipe for low hysteresis hydrophobic surfaces. *Faraday Discuss.* **146**, 103–111.
- [24] ERAL, H. B. & 'T MANNETJE, D. J. C. M. & OH, J. M. 2013 Contact angle hysteresis: a review of fundamentals and applications. *Colloid Polym Sci* **291**, 247–260.
- [25] DELSHAD, M. & NAJAFABADI, N. F. & ANDERSON, G. A. & POPE, G. A. & SEPEHRNOORI, K. 2009 Modeling Wettability Alteration by Surfactants in Naturally Fractured Reservoirs. *SPE J.* **12**, 361–370.

- [26] LASHGARI, H. R. & XU, Y. & SEPEHRNOORI, K. 2016 Modelling dynamic wettability alteration effect based on contact angle. *SPE*, 1–17.
- [27] ANDERSEN, P. Ø. & EVJE, S. & KLEPPE, H. & SKJÆVELAND, S. M. 2015 A Model for Wettability Alteration in Fractured Reservoirs. *SPE J.* **20**, 1261–1275.
- [28] ADIBHATIA, B. & SUN, X. & MOHANTY, K. 2005 Numerical Studies of Oil Production from Initially Oil-Wet Fracture Blocks by Surfactant Brine Imbibition. *SPE*, 1-15.
- [29] AL-MUTAIRI, S. M. & ABU-KHAMSIN, S. A. & HOSSAIN, M. E. 2012 A Novel Approach to Handle Continuous Wettability Alteration during Immiscible CO₂ Flooding Process. *SPE*, 1-12.
- [30] BARTLEY, J. T. & RUTH, D. W. 1999 Relative Permeability Analysis of Tube Bundle Models. *Transport porous med* **36**, 161–187.
- [31] HELLAND, J. O. & SKJÆVELAND, S. M. 2006 Physically based capillary pressure correlation for mixed-wet reservoirs from a bundle-of-tubes model. *SPE*, **11**, 171–180.
- [32] DONG, M. & DULLIEN, F. A. L. & DAI, L. & LI, D. 2005 Immiscible Displacement in the Interacting Capillary Bundle Model Part I. Development of Interacting Capillary Bundle Model. *Trends Anal. Chem.* **59**, 1–18.
- [33] SKJÆVELAND, S. M. & SIQVELAND, L. M. & KJOSAVIK, A. & THOMAS, W. L. H. & VIRNOVSKY, G. A. 2000 Capillary pressure correlation for mixed-wet Reservoirs. *SPE*, 60–67.
- [34] XU, W. S. & LUO, P. Y. & SUN, L. & LIN, N. 2016 A Prediction model of the capillary pressure J-function. *Plos One* **11**, 1–9.
- [35] FALODE, O. & MANUEL, E. 2014 Wettability effects on capillary pressure, relative permeability, and irreducible saturation using porous plate. *Journal of Petroleum Engineering* **2014**1–12.
- [36] AHMED, A. & PATZEK, T. W. 2003 The Impact of Wettability Alteration on Two-Phase Flow Characteristics of Sandstones-A Quasi-Static Description. *Water Resources Research* **39**1-10.
- [37] BOBEK, J. E. & MATTAX, C. C. & DENEKAS, M. O. 1958 Reservoir Rock Wettability-Its Significance and Evaluation. *SPE* **213**155–160.
- [38] ANDERSON, W. 1939 Wettability Literature Survey-Part 5: The Effects of Wettability on Relative Permeability. *Journal of Petroleum Technology* **39** 1453–1468.
- [39] PENTLAND, C. H. & EL-MAGHRABY, R. & IGLAUER, S. & BLUNT, M. J. 2011 Measurements of the capillary trapping of super-critical carbon dioxide in Berea sandstone. *Geophys. Res. Lett.* **38**1-4.
- [40] IGLAUER, S. & PALUSZNY, A. & PENTLAND, C. H. & BLUNT, M. J. 2011 Residual CO₂ imaged with Xray microtomography. *Geophys. Res. Lett.* **38** 1-6.
- [41] SALATHIEL, R. A. 1973 Oil recovery by surface film drainage in mixed-wettability rocks. *J. Petrol. Technol.* **25** 1216–1224.
- [42] TREIBER, L. E. & ARCHER, D. L. & OWENS, W. W. 1972. A laboratory evaluation of the wettability of fifty oil-producing reservoirs. *SPE J.* **12** 531–540.

- [43] MORROW, N. R. 1970 Physics and thermodynamics of capillary action in porous media. *Ind. Eng. Chem.* **62** 32-56.
- [44] ANDERSON, W. G. 1986 Wettability literature survey—Part 1: Rock/oil/brine interactions and the effects of core handling on wettability. *J. Pet. Tech.* **38** 1125–1144
- [45] WANG, S. & EDWARDS, I. M. & CLARENS, A. F. 2013 Wettability phenomena at the CO₂-brine-mineral interface: Implications for geologic carbon sequestration. *Environ Sci Technol* **47** 234-241.
- [46] BIKKINA, P. K. 2011 Contact angle measurements of CO₂-water-quartz/calcite systems in the perspective of carbon sequestration. *Int. J. Greenhouse Gas Control* **5** 1259-1271.
- [47] YANG, D. D. & GU, Y. G. & TONTIWACHWUTHIKUL, P. 2008 Wettability determination of the reservoir brine-reservoir rock system with dissolution of CO₂ at high pressures and elevated temperatures. *Energy Fuels* **22** 504–509.
- [48] DICKSON, J. L. & GUPTA, G. & HOROZOV, T. S. & BINKS, B. P. & JOHNSTON, K. P. 2006 Wetting phenomena at the CO₂/water/glass interface. *Langmuir* **22** 2161–2170.
- [49] IGLAUER, S. & MATHEW, M. & BRESME, F. 2012 Molecular dynamics computations of brine-CO₂ interfacial tensions and brine-CO₂-quartz contact angles and their effects on structural and residual trapping mechanisms in carbon geosequestration. *J. Colloid Interface Sci.* **386** 405–414.
- [50] JUNG, J. W. & WAN, J. 2012 Supercritical CO₂ and ionic strength effects on wettability of silica surfaces: Equilibrium contact angle measurements. *Energy Fuels* **26** 6053–6059.
- [51] ESPINOZA, D. N. & SANTAMARINA, J. C. 2010 Water-CO₂-mineral systems: Interfacial tension, contact angle, and diffusion Implications to CO₂ geological storage. *Water Resour Res.* **46** 1-10.
- [52] FAROKHPOOR, R. B. & BJØRKVIK, J. A. & LINDEBERG, E. & TORSÆTER, O. 2013 Wettability behaviour of CO₂ at storage conditions. *Int. J. Greenhouse Gas Control* **12** 18–25.
- [53] SARAJI, S. & GOUAL, L. & PIRI, M. & PLANCHER, H. 2013 Wettability of ScCO₂/Water/Quartz Systems: Simultaneous Measurement of Contact Angle and Interfacial Tension at Reservoir Conditions. *Langmuir* 1-39.
- [54] KOVSEK, A. R. & WONG, H. & RADKE, C. J. 1993 A pore-level scenario for the development of mixed wettability in oil reservoirs. *AIChE J.* **39**, 1072–1085.
- [55] POWERS, S. E. & ANCKNER, W. H. & SEACORD, T. F. 1996 Wettability of NAPL-contaminated sands. *J. Environ. Eng.* **122** 889–896.
- [56] VIVES, M. & CHANG, Y. & MOHANTY, K. 1999 Effect of Wettability on Adverse-Mobility Immiscible Floods. *SPE J.* **4**. 260–267.
- [57] DELSHAD, M. & LENHARD, R.J. & OOSTROM, M. & POPE, G.A. 2003 A Mixed-Wet Hysteretic Relative Permeability and Capillary Pressure Model for Reservoir Simulations. *SPE Reservoir Evaluation and Engineering* **6**. 328–334.

- [58] SPITERI, E. J. & JUANES, R. & BLUNT, M. J. & ORR, F. M. 2008 A New Model of Trapping and Relative Permeability Hysteresis for All Wettability Characteristics. *J. SPE J.* **13** 277–288.
- [59] LANDRY, C. J. & KARPYN, Z. T. & AYALA, O. 2014 Relative permeability of homogenous-wet and mixed-wet porous media as determined by pore-scale lattice Boltzmann modeling. *Water Resour. Res.* **50** 3672–3689.
- [60] KJOSAVIK, A. & RINGEN, J. K. & SKJÆVELAND, S. M. 2002 Relative Permeability Correlation for Mixed-Wet Reservoirs. *SPE J* **7** 49–58.
- [61] LOMELAND, F. & EBELTOFT, E. & HAMMERVOLD, T. W. 2005 A new versatile relative permeability correlation. *Society of Core Analysts*.
- [62] SEDAGHAT, M. H. & AZIZMOHAMMADI, S. 2019 Dynamic wettability alteration in naturally fractured rocks. *Comput Geosci* 1-11.
- [63] BROOKS, R. H. & COREY, A. T. 1964 Hydraulic properties of porous media. **7** 26-28.
- [64] VAN GENUCHTEN, M. T. 1980 A closed-form equation for predicting the hydraulic conductivity of unsaturated soils. *Soil Sci Soc Am J* **44** 892–898
- [65] KASSA, A. M. & GASDA, S. E. & KUMAR, K. RADU, F. A. 2020 Impact of Time-Dependent Wettability Alteration on the Dynamics of Capillary Pressure. *Adv Water Resour* **142**.
- [66] LI, K. & HORNE, R. N. 2006 Comparison of methods to calculate relative permeability from capillary pressure in consolidated water-wet porous media. *Water Resour. Res.* **42** 1-9.
- [67] HUI, M. & BLUNT, M. J. 2000 Effects of Wettability on Three-Phase Flow in Porous Media. *J. Phys. Chem. B* **104**, 3833–3845.
- [68] WASHBURN, E. 1921 The dynamics of capillary flow. *Phys. Rev* **7** 273–283.
- [69] HELLAND, J. O. & SKJÆVELAND, S. M. 2007 Relationship between capillary pressure, saturation, and interfacial area from a model of mixed-wet triangular tubes. *WATER RESOURCES RESEARCH*. **43** 1-15.
- [70] BRADFORD, S. A. & LEIJ, F. J. 1997 Estimating interfacial areas for multi- fluid soil systems. *J. Contam. Hydrol.* **27** 83–105.
- [71] VAN DIJKE, M. I. J. & SORBIE, K. S. 2006 Existence of fluid layers in the corners of a capillary with non-uniform wettability, *Journal of Colloid and Interface Science*, **293** 455–463
- [72] HELLAND, J. O. & SKJÆVELAND, S. M. 2006
- [73] Physically based capillary pressure correlation for mixed-wet reservoirs from a bundle-of-tubes model. *SPE J.* 171–180.
- [74] Effect of contact angle on drainage and imbibition in regular polygonal tubes. MA, S. & MASON, G. & MORROW, N. R. 1996 *Colloids and Surfaces* **117** 273–291.
- [75] JAFARI, M. & JUNG, J. 2016 The change in contact angle at unsaturated CO₂-water conditions: Implication on geological carbon dioxide sequestration. *Geochem. Geophys. Geosyst.* **17** 3969–3982

- [76] MORTON III, S. A. & KEFFER, D. J. & COUNCE, R. M. & DEPAOLI, D. W. & HU M. Z. C. 2004 Thermodynamic method for prediction of surfactant-modified oil droplet contact angle. *Journal of Colloid and Interface Science* **270** 229–241,
- [77] DAVIS, A.N. & MORTON III, S. A. & COUNCE, R.M. & DEPAOLI, D.W. & HU, M.Z.-C. 2003 Ionic strength effects on hexadecane contact angles on a gold-coated glass surface in ionic surfactant solutions. *Colloids Surf. A* **221** 69–80.